CHAPTER 11

DIFFUSION-TENSOR MR IMAGING FUNDAMENTALS

Peter J. Basser

INTRODUCTION

It is remarkable that the MR measurement of the diffusivity of water in neural tissue provides unique and useful biological and clinical information about tissue composition, the physical properties of its constituents, tissue microstructure, and architectural organization. Moreover, this information can be obtained in vivo, noninvasively without contrast agents.

This chapter deals with diffusion-tensor MRI, which provides new information about tissue microstructure, particularly anisotropic tissues like brain white matter, beyond that provided by diffusion-weighted MRI and conventional diffusion MRI.

What is diffusion anisotropy? It is simply that the measured apparent diffusion coefficient (ADC) is not the same in all directions, i.e. it is not directionally uniform (isotropic) as in a jar of water. The observation of diffusion anisotropy in tissues is usually a clue that the underlying microstructure is ordered. Characterizing diffusion anisotropy quantitatively can provide information not only about the alignment direction, but also often about the organization and properties of the ordered elements.

In a biological context, anisotropic diffusion was first observed in NMR experiments with skeletal muscle.[1,2] Interest in the phenomenon, however, was rekindled when it was observed in MRIs of animal and human brains.[3-7]

DIFFUSION AND DIFFUSION-TENSOR MRI

Other chapters in this book explain diffusion MRI, its underpinnings and its applications. There is no need to repeat this information here. It will be assumed the reader is familiar with the notion of a diffusion-weighted image (DWI) as well as conventional MRI pulse sequences used to acquire one. Familiarity with the formula used to calculate an ADC in each voxel from a set of DWIs is also assumed. The notion of the b-factor or b-value has also been introduced in this context as a measure of the degree of diffusion weighting.

A reasonable starting point is to compare and contrast diffusion MRI (DI) and diffusion tensor MRI (DTI), which is sometimes referred to as DT-MRI.[8] DI is based upon a one-dimensional Gaussian model of molecular displacements. The measurement of an ADC is obtained from analyzing the projection of all molecular displacements along one direction. In tissues, such as brain gray matter, where the ADC is largely independent of the orientation of the tissue, a single ADC is often sufficient to characterize the diffusion process at the voxel scale. However, in anisotropic media, such as skeletal and cardiac muscle[1,2,9] and in white matter,[5,10-12] where the ADC depends upon the orientation of the tissue, the 1-D Gaussian model is inadequate to characterize the orientation-dependent water mobility.

A more general description of anisotropic free diffusion uses a three-dimensional Gaussian model of molecular displacements. This model contains a symmetric effective or apparent diffusion tensor of water, $\underline{D}$ (e.g. see reference 13) to describe the orientation dependence of diffusion instead of a scalar diffusion coefficient.

In essence, DTI consists of the measurement of $\underline{D}$ (and functions of it) from a series of DWIs. $\underline{D}$ is determined by using a relationship between the measured echo signal in each voxel and the applied magnetic field gradient sequence,[14-17] which was derived from Stejskal's classic solution to the modified Bloch-Torrey equation[18]:

$$\ln\left(\frac{A(\underline{b})}{A(\underline{b}=\underline{0})}\right) = -\left(b_{xx}D_{xx} + 2b_{xy}D_{xy} + 2b_{xz}D_{xz} + b_{yy}D_{yy} + 2b_{yz}D_{yz} + b_{zz}D_{zz}\right) \quad \text{(Eq. 11-1)}$$

Above, $A(\underline{b})$ is the echo magnitude of the diffusion-weighted signal, $A(\underline{b}=\underline{0})$ is the echo magnitude of the nondiffusion-weighted signal, and b_{ij} is a component of the symmetric b-matrix, $\underline{b}$. In DI a scalar b-factor is calculated for each DWI; in DTI a symmetric b-matrix is calculated for each DWI. Whereas the b-value summarizes the attenuating effect of diffusion and imaging gradients on the MR signal along one direction,[19] the b-matrix summarizes the attenuating effect of all gradient waveforms (i.e., all imaging and diffusion gradient sequences) applied in all three directions, x, y, and z.[14-17] Just as in DI, each DWI is used with its corresponding b-factor to estimate an ADC using linear regression; in DTI, each DWI is used with its corresponding b-matrix to estimate $\underline{D}$ using multivariate linear regression of Eq.11-1. Multivariate linear regression is just one of a number of techniques, including nonlinear regression and singular-value decomposition, that could be used to estimate $\underline{D}$ from the echo data.

In the limiting case in which the medium is isotropic, it is easy to show that the 3-D Gaussian model assumed in DTI reduces to the 1-D Gaussian model assumed in DI. To see this, set $D_{xx} = D_{yy} = D_{zz} = D$, and $D_{xy} = D_{xz} = D_{yz} = 0$. Then, Equation 11-1 reduces to:

$$\ln\left(\frac{A(\underline{b})}{A(\underline{b}=\underline{0})}\right) = -bD$$

$$\text{with} \qquad b = b_{xx} + b_{yy} + b_{zz} = \text{Trace}(\underline{b}). \quad \text{(Eq. 11-2)}$$

There are two important differences between the designs of DI and DTI experiments. First, in DTI diffusion gradients must be applied along at least six noncolinear directions,[14] whereas in DI it is sufficient to apply diffusion gradients along only one direction. Second, the notion of "cross-terms" must be expanded in DTI. Interactions between imaging and diffusion gradients applied in orthogonal directions, and even between imaging gradients applied in orthogonal directions, can introduce additional diffusion weighting.[15,16] It can be seen from Equation 11-2 that diffusion weighting can be introduced by imaging (e.g., slice select gradients) applied along the x, y, or z directions. In isotropic media, however, interactions between gradients applied in orthogonal directions do not produce any diffusion attenuation, but in anisotropic media these interactions can result in diffusion attenuation.

It is important to note that MRI measurements of the ADC, T1, T2, MT, proton density, phase, and chemical shift were all preceded by classical NMR measurements of these quantities, which in some cases were introduced almost a half century before their MRI counterpart. For DTI, however, there was no classical NMR method developed either to measure the self-diffusion tensor or the effective (or apparent) diffusion tensor of water (or other species) in the laboratory coordinate frame. So, unlike T1 MRI or DI, implementing DTI first required the developing of a new method to measure $\underline{D}$ using NMR means[14,20] and then combining it with conventional MRI.[8]

GEOMETRIC REPRESENTATION OF TRANSLATIONAL DIFFUSION IN 3-D

The most intuitive way to understand what $\underline{D}$ means is by considering a Gedanken experiment in which the Brownian motion of an ensemble of "tagged" water molecules released from the center of a voxel is followed, as depicted in Figure 11-1. If this experiment is performed in a jar of water, then the rate of diffusive transport is the same in all directions. Diffusion is said to be isotropic and is completely specified by a single scalar constant, D, the diffusion coefficient. Thus, diffusion

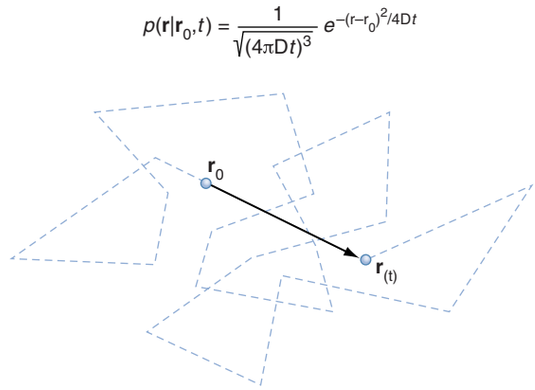

$p(\mathbf{r}|\mathbf{r}_0,t)$ is the probability of finding a particle at position $\mathbf{r}$, and at a time t, given a starting position $\mathbf{r}_0$, and at a time 0.

FIGURE 11-1

The Brownian picture of diffusion is best epitomized by illustrating a possible path taken by a molecule that is released at point $\mathbf{r}_0$ at time t=0 and moves to position $\mathbf{r}$ at a later time, t. The molecule undergoes a "drunk walk" whose random motion is described by a displacement probability distribution.

isotropy describes the case in which the molecular diffusivity is independent of the medium's orientation. For a diffusion time, Δ, the translational displacement distribution is spherically symmetric, and surfaces of constant probability or water concentration are concentric spheres. When considering the Einstein formula for 1-D diffusion[21]:

$$< r^2 > = 2D\Delta \qquad \text{(Eq. 11-3)}$$

it is possible to construct a particular sphere whose radius equals the root mean-squared (rms) displacement of water molecules after diffusion time Δ, a graphical representation of which can be found in Figure 11-2A.

If the Gedanken experiment is performed in a liquid crystal or system with microscopic aligned rods, then the rate of diffusive transport will no longer be the same in all directions. Diffusion anisotropy implies that the translational displacement probability of the diffusing species now depends upon the medium's orientation. In homogeneous (i.e., spatially uniform) anisotropic media, the voxel-averaged displacement distribution is given by:

$$P(\mathbf{r}, \Delta|\mathbf{0}, 0) = \frac{1}{\sqrt{|\underline{D}|(4\pi\Delta)^3}}\, e^{\frac{-\mathbf{r}^T\, \underline{D}^{-1}\, \mathbf{r}}{4\Delta}} \qquad \text{(Eq. 11-4)}$$

where the column vector $\mathbf{r} = (x,y,z)^T$ is the net displacement, and $|\underline{D}|$ is the determinant of $\underline{D}$. The covariance matrix, $2\Delta\,\underline{D}$, characterizes the width of the distribution, which changes with orientation. Now, when surfaces of constant probability or particle concentration are constructed by setting the exponent in Equation 11-4 to a constant, then we obtain:

$$(Dyy\ Dzz - Dyz^2)\,x^2 + 2\,(Dxz\ Dyz - Dxy\ Dzz)\,x\,y + (Dxx\ Dzz - Dxz^2)\,y^2 + 2\,(Dxy\ Dyz - Dxz\ Dyy)\,x\,z + 2\,(Dxy\ Dxz - Dxx\ Dyz)\,y\,z + (Dxx\ Dyy - Dxy^2)\,z^2 = |\underline{D}|\Delta \qquad \text{(Eq. 11-5A)}$$

that can be rewritten as:

$$a\,x^2 + 2\,b\,x\,y + d\,y^2 + 2\,c\,x\,z + 2\,e\,y\,z + f\,z^2 = 1\ , \qquad \text{(Eq. 11-5B)}$$

This equation represents a three-dimensional ellipsoid,* called the "diffusion ellipsoid".[8,13,22] This is shown in Figure 11-2B. The six independent parameters (a,b,c,d,e,f) in Equation 11-5b contain all information required to specify the *size, shape,* and *orientation* of this ellipsoid. Not coincidentally the number of independent elements of $\underline{D}$ required to specify the form of the three-dimensional displacement distribution in Equation 11-4 is also six.

The laboratory (x-y-z) coordinate axes can always be rotated so that they are aligned with the local principal (x'-y'-z') axis of the diffusion ellipsoid in each voxel. In the preferred principal frame, all off-diagonal elements of $\underline{D}$ vanish; Equation 11-5A simplifies to:

$$\left(\frac{x'}{\sqrt{2\lambda_x'\Delta}}\right)^2 + \left(\frac{y'}{\sqrt{2\lambda_y'\Delta}}\right)^2 + \left(\frac{z'}{\sqrt{2\lambda_z'\Delta}}\right)^2 = 1\ . \qquad \text{(Eq. 11-6)}$$

Above λ_x', λ_y', and λ_z' are the three principal diffusivities (or eigenvalues), corresponding to the three respective principal directions, $\varepsilon_{x'}$, $\varepsilon_{y'}$, $\varepsilon_{z'}$; $\sqrt{2\lambda_x'\Delta}$, $\sqrt{2\lambda_y'\Delta}$, and $\sqrt{2\lambda_z'\Delta}$ are the root mean-squared (rms) displacements along these three principal directions at diffusion time Δ, respectively. The lengths of the major and minor axes of the diffusion ellipsoid represent these three distances. Note that the direction of the principal (x'-y'-z') axes of the diffusion ellipsoid are generally not known a priori, and typically do not coincide with the laboratory coordinate axes. It is necessary to assume that they are different in each voxel.[14] An example of an in vivo diffusion ellipsoid image is shown in Figure 11-3.

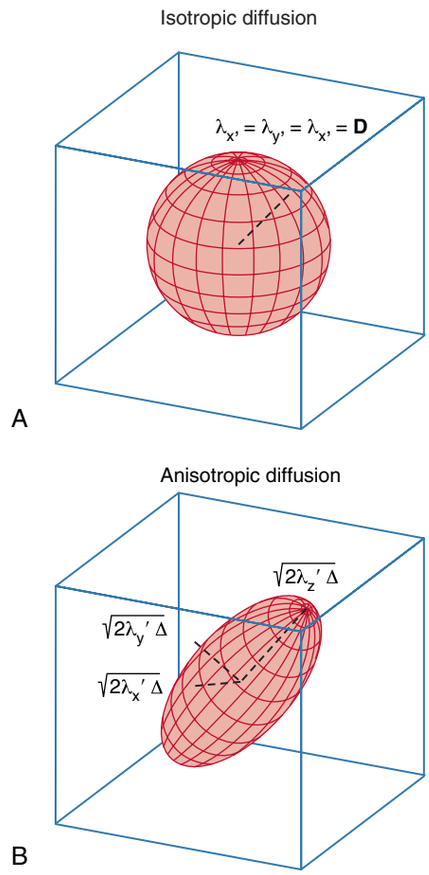

FIGURE 11-2

A, In isotropic media, the rms displacement or diffusion ellipsoid is spherical. **B,** However, in anisotropic media, the diffusion ellipsoid can be prolate or oblate, and its three principal directions are coincident with the eigenvectors of $\underline{D}$, ε_1, ε_2, and ε_3.

*This is true because both $\underline{D}$ and the matrix of coefficients, $\begin{pmatrix} a & b & c \\ b & d & e \\ c & e & f \end{pmatrix}$ are positive definite.

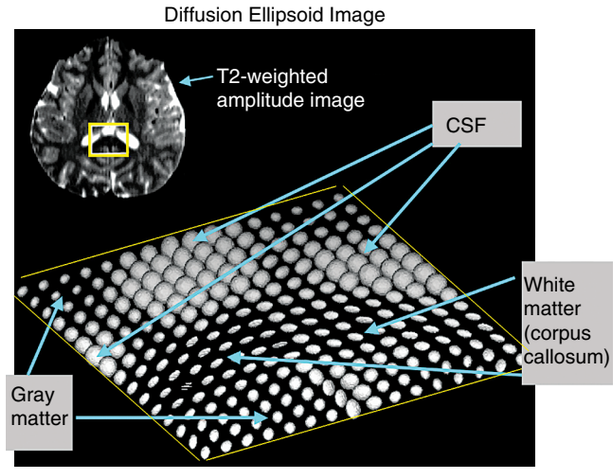

FIGURE 11-3

The T2-weighted axial image contains an ROI encompassing the lateral ventricles and corpus callosum. A diffusion ellipsoid image constructed from each voxel within the ROI shows the size, shape and orientation of the diffusion ellipsoid. CSF is clearly depicted by large spherical ellipsoids in which diffusion is free and isotropic. Gray matter is depicted by smaller spherical ellipsoids, indicating isotropic diffusion but lower mean diffusivity than in the CSF. White matter is depicted by prolate diffusion ellipsoids whose polar axis is aligned with the purported white matter fiber direction in the corpus callosum. *(From Pierpaoli C, Jezzard P, Basser PJ, et al: Diffusion tensor MR imaging of the human brain. Radiology 201:637-648, 1996.)*

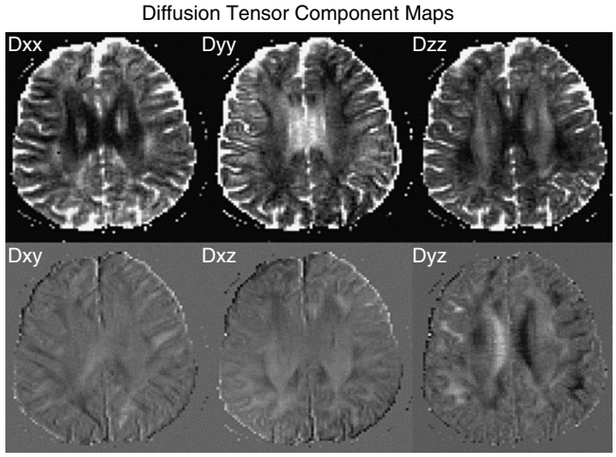

FIGURE 11-4

DTI provides data for each slice within the imaging volume that consists of images of the three diagonal elements of $\underline{D}$ (top row), and of the three off-diagonal elements of $\underline{D}$ (bottom row). *(From Pierpaoli C, Jezzard P, Basser PJ, et al: Diffusion tensor MR imaging of the human brain. Radiology 201:637-648, 1996.)*

In summary, both diagonal and off-diagonal elements of $\underline{D}$ measured in DTI, maps of which are shown in Figure 11-4, are essential in specifying the probability distribution in Equation 11-4 as well as in characterizing the size, shape, and orientation of the diffusion ellipsoid constructed from $\underline{D}$ in each voxel.

QUANTITATIVE PARAMETERS PROVIDED BY DTI

Scalar parameters that embody distinct intrinsic features listed earlier in italics can be displayed as an image. Parameters describing the size and shape of the ellipsoid should be rotationally invariant, i.e., independent of the orientations of the anisotropic structure, patient's body within the MR magnet, the applied diffusion sensitizing gradients, and choice of the laboratory coordinate system in which the components of $\underline{D}$ and the magnet field gradients are measured.[23,24]

Possibly the most important quantitative scalar parameters provided by DTI are the three sorted eigenvalues, λ_1, λ_2, and λ_3 (i.e., the eigenvalues of $\underline{D}$ described above, λ_x',λ_y', and λ_z', but sorted according to size). An example of an eigenvalue image is shown in Figure 11-5. Combinations of these quantities are used to characterize the size and shape of the diffusion ellipsoid. The orientational information is encoded by the three eigenvectors of $\underline{D}$.

SIZE OF DIFFUSION ELLIPSOID

Quantities described later characterize the size of the diffusion ellipsoid, independent of orientation and shape:

$$\begin{aligned} \text{Trace}(\underline{D}) &= D_{xx} + D_{yy} + D_{zz} = 3\langle D\rangle \\ &= \lambda_1 + \lambda_2 + \lambda_3 = 3\langle\lambda\rangle \end{aligned} \qquad \text{(Eq. 11-7)}$$

Physically, Trace($\underline{D}$) is three times the orientationally averaged diffusivity, <D>, which can be obtained by arithmetically averaging the ADC distribution uniformly over all possible directions.[25] Trace($\underline{D}$) measures an intrinsic property of the tissue, which is independent of fiber orientation, gradient directions, etc. An example of a Trace($\underline{D}$) image of brain parenchyma is provided in Figure 11-6.

What is the clinical value of Trace($\underline{D}$)? Moseley et al. discovered in animals,[26-28] and Warach et al. later showed in humans[29,30] that a reduction of the ADC in brain parenchyma sensitively indicates the onset and severity of a cerebral ischemic event. Moreover, an elevation in ADC was observed in chronic stroke, often leading to lacunar infarcts. Thus, it seemed possible to follow an acute stroke in progress, and the subsequent chronic degeneration it caused using the ADC. However, this aim was hampered by anisotropic diffusion observed in white matter. There, DWI intensity and the ADC depend on the direction of the diffusion sensitizing gradient with respect to the white matter fiber orientation.[3,11,31] Thus, it was generally not possible to determine whether an observed drop or recovery in the DWI or ADC was of a physiological origin (brought on by the ischemic event itself) or arose because of the relative orientation of the white matter tracts and the applied diffusion gradient. In ischemia monitoring applications, diffusion anisotropy

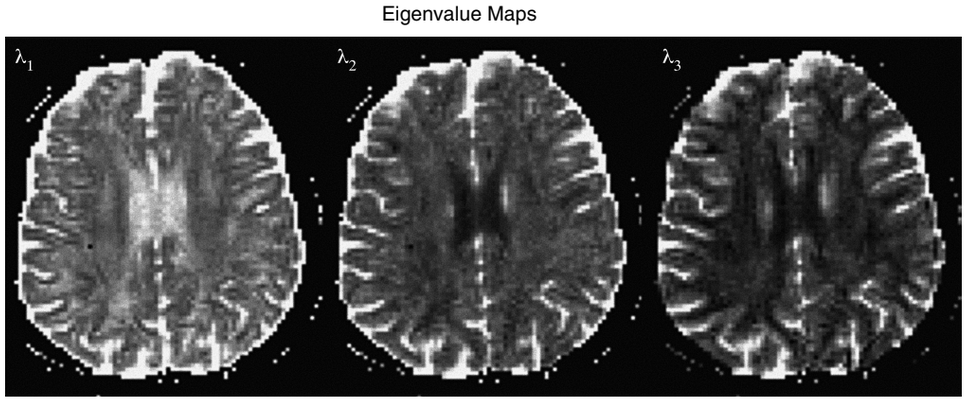

FIGURE 11-5

Images or maps of the three sorted eigenvalues, λ_1, λ_2, and λ_3. Different regions of brain can be distinguished by examining these images. CSF is uniformly bright in these images, indicating diffusion is isotropic and high there. Grey matter regions are nearly uniform in brightness, while white matter regions, like the corpus callosum at the center, is bright in the λ_1 image but dark in the λ_2 and λ_3 images, indicating significant diffusion anisotropy there. *(From Pierpaoli C, Jezzard P, Basser PJ, et al: Diffusion-tensor MR imaging of the human brain. Radiology 201:637-648, 1996.)*

in white matter produced directionally dependent intensity variations in DWIs and in ADC maps that complicated their interpretation, and was considered by many to be a confounding artifact.

The solution to this vexing problem was provided by DTI. Unlike the DWI signal intensity and the ADC, Trace(D) is inherently insensitive to both the direction of the diffusion sensitizing gradient and of the orientation of white matter in a voxel.[23] Thus, displaying Trace(D) or <D> instead of the ADC eliminates all orientational dependence seen in DWIs and ADC maps, so changes in signal can be ascribed solely to changes in the tissue's physiologic state.

The use of <D> in acute and chronic stroke assessment is probably the most important current clinical application of DTI, although it is not widely known that Trace(D) and <D> (sometimes referred to as the "mean ADC") are actually diffusion–tensor-derived parameters. A second reason for the success of DTI in stroke assessment (and other brain disorders) is the surprising finding that in normal brain parenchyma Trace(D) is highly uniform.[32-35] Remarkably, it has virtually the same value in both white and gray matter. Van Gelderen, et al[35] first demonstrated in cats, and Ulug et al[34] in humans that an image of Trace(D) (or of <D>) defines ischemic regions better than the corresponding DWI or ADC map.

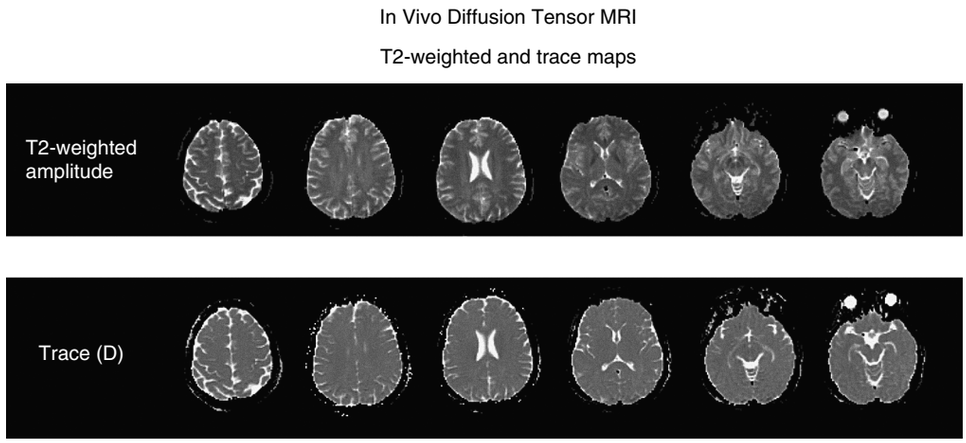

FIGURE 11-6

T2-weighted amplitude images (top row) and Trace(D) maps (bottom row) obtained for the same slice. Trace(D) images are remarkably uniform in normal brain parenchyma. Hyperintense regions correspond to CSF or fluid-filled regions. *(From Pierpaoli C, Jezzard P, Basser PJ, et al: Diffusion tensor MR imaging of the human brain. Radiology 201:637-648, 1996.)*

Several MR sequences have been proposed to produce a "trace-weighted" or "isotropically weighted" MRI. Clever schemes were proposed by Wong et al. and Mori et al. that use only two DWIs.[36,37] One way to compute a trace-weighted image is to compute <D> and then to generate an image whose intensity is a function of it, such as exp(–*b* <D>) where *b* is defined in Equation 11-2. In such an image, ischemic regions would appear bright while normal parenchyma appears dark. A general formalism for producing trace-weighted images from a set of DWIs can be found in reference 38.

SHAPE OF DIFFUSION ELLIPSOID

Characterizing the degree of diffusion anisotropy is tantamount to characterizing the shape of the three-dimensional diffusion ellipsoid, independent of its orientation and size. Such a measure should also be rotationally invariant, i.e., independent of the sample's placement or its orientation with respect to the (laboratory) x-y-z reference frame.[8] One way of deriving these parameters is by analyzing the anisotropic part of the $\underline{D}$ or the "diffusion deviation tensor" in each voxel, $\underline{D}$[39,40]:

$$\underline{D} = \underline{D} - \langle D \rangle \underline{I} \qquad \text{(Eq. 11-8)}$$

where above, the familiar mean diffusivity, <D>, is seen, multiplied by the identity tensor, $\underline{I}$. In defining the deviation tensor, the part of $\underline{D}$ that is isotropic is simply subtracted off. What remains is the anisotropic part of $\underline{D}$. The magnitude of the diffusion deviation tensor, Trace($\underline{D}^2$), can be shown to be proportional to the sample variance of the eigenvalues or principal diffusivities[39]:

$$\begin{aligned} &1/3\,\mathrm{Trace}(\underline{D}^2) \\ &= \frac{(\lambda_1 - \langle\lambda\rangle)^2 + (\lambda_2 - \langle\lambda\rangle)^2 + (\lambda_3 - \langle\lambda\rangle)^2}{3} \\ &= \mathrm{Var}(\boldsymbol{\lambda}) \end{aligned} \qquad \text{(Eq. 11-9)}$$

This quantity, which is rotationally invariant, is used in several popular diffusion anisotropy measures, such as the Relative Anisotropy (*RA*)[39]:

$$RA = \frac{\sqrt{Var(\lambda)}}{\langle D \rangle} \qquad \text{(Eq. 11-10)}$$

and the Fractional Anisotropy (*FA*)[39]:

$$FA = \frac{3}{\sqrt{2}} \frac{\sqrt{Var(\lambda)}}{\sqrt{\lambda_1^2 + \lambda_2^2 + \lambda_3^2}} \qquad \text{(Eq. 11-11)}$$

Both characterize the degree of "out-of-roundness" of the diffusion ellipsoid. The *RA* is just the coefficient of variation of the eigenvalues. The *FA* measures the fraction of the magnitude of the diffusion tensor that is anisotropic.[39] An example of a whole-brain *FA* map is provided in Figure 11-7. Other anisotropy measures have also been proposed, some differing from the *FA* and *RA* above by only a scale factor.[41]

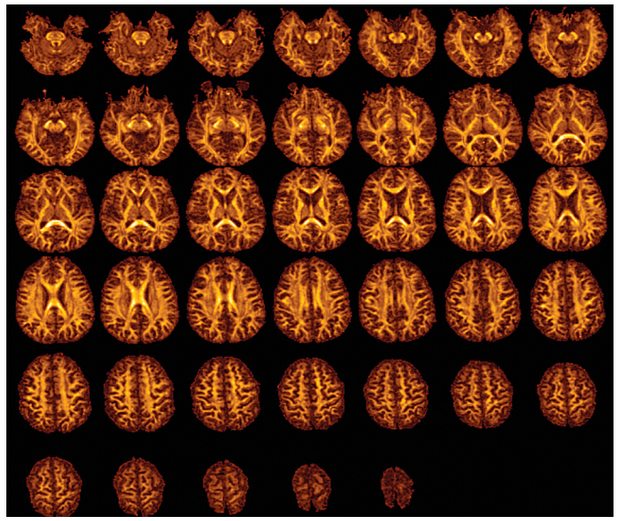

FIGURE 11-7

Whole-brain axial slices showing the distribution of *FA*. *(Courtesy of Derek Jones.)*

Another useful "shape" parameter is the third moment or skewness of the eigenvalues:

$$\begin{aligned} &1/3\,\mathrm{Trace}(\underline{D}^3) \\ &= \frac{(\lambda_1 - \langle\lambda\rangle)^3 + (\lambda_2 - \langle\lambda\rangle)^3 + (\lambda_3 - \langle\lambda\rangle)^3}{3} \\ &= \mathrm{Skewness}(\boldsymbol{\lambda}) \end{aligned} \qquad \text{(Eq. 11-12)}$$

When the skewness is positive the diffusion ellipsoid is prolate (i.e., cigar shaped—a shape observed in white matter fibers in the corpus callosum and in the pyramidal tract in monkeys[32] and in humans[33]). When it is negative, the diffusion ellipsoid is oblate (i.e., pancake shaped—a shape observed in white matter in the subcortical white matter regions in the centrum semiovale in humans[33]). Clearly, it would be useful to determine higher moments of the distribution of eigenvalues of $\underline{D}$, such as the Kurtosis(λ), in order to characterize diffusion anisotropy more completely, however, typically noise in DWIs introduces enough bias in the estimates of the eigenvalues to make these higher-order statistics inaccurate. Background noise even causes overestimation of the variance of the eigenvalues, and other measures of diffusion anisotropy due to a phenomenon called "eigenvalue repulsion".[32]

Three novel tensor-derived parameters have been proposed that measure the degree to which $\underline{D}$ is line-like, plane-like, and sphere-like (corresponding to diffusion ellipsoids that are prolate, oblate, and spherical, respectively).[42] This tensor decomposition provides a useful and different geometric interpretation of the diffusion process. These diffusion measures, however, are

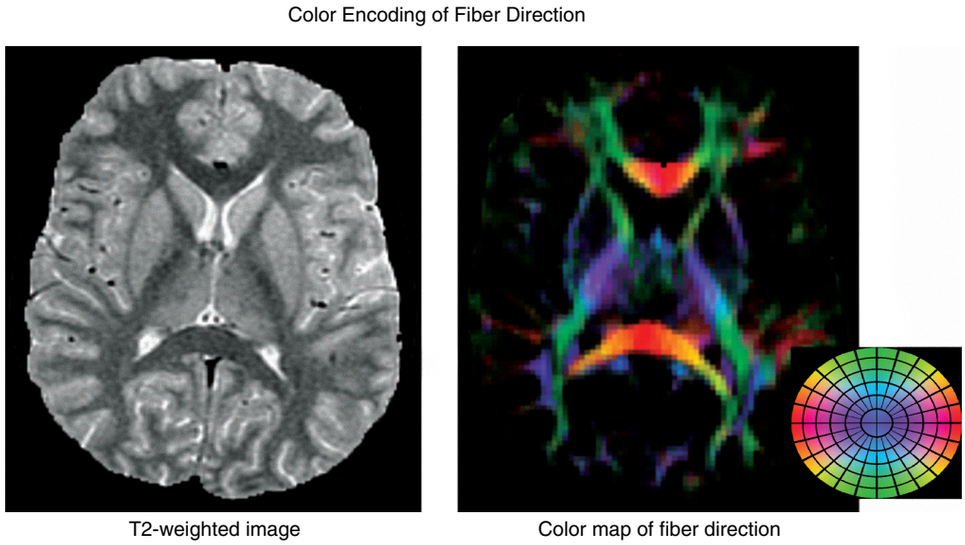

FIGURE 11-8

A T2-weighted image juxtaposed with a direction-encoded color map. This color scheme overcomes the problem of using line drawings to depict fiber orientation within a voxel, since all fibers can be perceived, and their orientations determined from the color wheel in the legend. *(From Pajevic S, Pierpaoli C. Color schemes to represent the orientation of anisotropic tissues from diffusion tensor data: application to white matter fiber tract mapping in the human brain. Magn Reson Med 42:526-540, 1999. Reproduced with permission of Wiley-Liss, Inc., a subsidiary of John Wiley & Sons, Inc.)*

not rotationally invariant (as are the three moments of D, the mean, variance, and skewness, described earlier), which could introduce additional statistical bias in their distributions (see Reference 32).

ORIENTATION OF DIFFUSION ELLIPSOIDS AND THEIR SPATIAL DISTRIBUTION

Another important development in DTI has been the introduction of quantities that reveal the distribution or spatial pattern of diffusion ellipsoids within an imaging volume. Some features involve the spatial rate of change of tensor-derived quantities within the imaging volume, such as the gradient of <D>, or the gradient of the magnitude of the deviation tensor described earlier.[43] The former provides information about the location of boundaries between cerebrospinal fluid (CSF) and tissue parenchyma, while the latter provides information about boundaries between white and gray matter. Typically, it is challenging to calculate these quantities from noisy, discrete, voxel-averaged DTI data, so some spatial smoothing for example, using a continuous approximation to the diffusion tensor field[43] or a regularization scheme,[44] must be performed beforehand.

Initially, it was proposed that in ordered fibrous tissues, the eigenvector associated with the largest eigenvalue within a voxel lies parallel to the local fiber direction.[8] Imaging methods that apply this idea include direction field mapping, in which the local fiber direction (or more correctly, orientation) is displayed as a vector (or line segment) in each voxel, and fiber-tract color mapping, in which a color, assigned to a voxel containing anisotropic tissue, is used to signify the local fiber tract direction (see Figure 11-8).[45] An important achievement of color mapping has been the ability to identify unambiguously all major commissural, association and projection pathways in the human brain[46,47] as shown in Figure 11-9.

DTI FIBER TRACTOGRAPHY

DTI fiber tractography is a natural extension of diffusion ellipsoid imaging. Re-examine the diffusion ellipsoid image containing the corpus collosum shown in Figure 11-3. Imagine now that adjacent, coherently ordered ellipsoids suggestive of a continuous fiber tract can be connected. What is obtained is an object like a link-sausage that represents a possible fiber tract. DTI fiber tractography[48-54] is the formal name given to this procedure in which coherently ordered fiber tract trajectories within the brain and other fibrous tissues are mathematically followed. Like color mapping, it is also based on the idea that in ordered fibrous tissues, the eigenvector associated with the largest eigenvalue within a voxel is parallel to the local fiber direction.[8] A nice review of this emerging field is given in reference 55.

Since its introduction, several different schemes have been proposed to follow fiber tracts. In the so-called "streamline" approaches, fiber-tract trajectories are generated from the local fiber tract direction field in

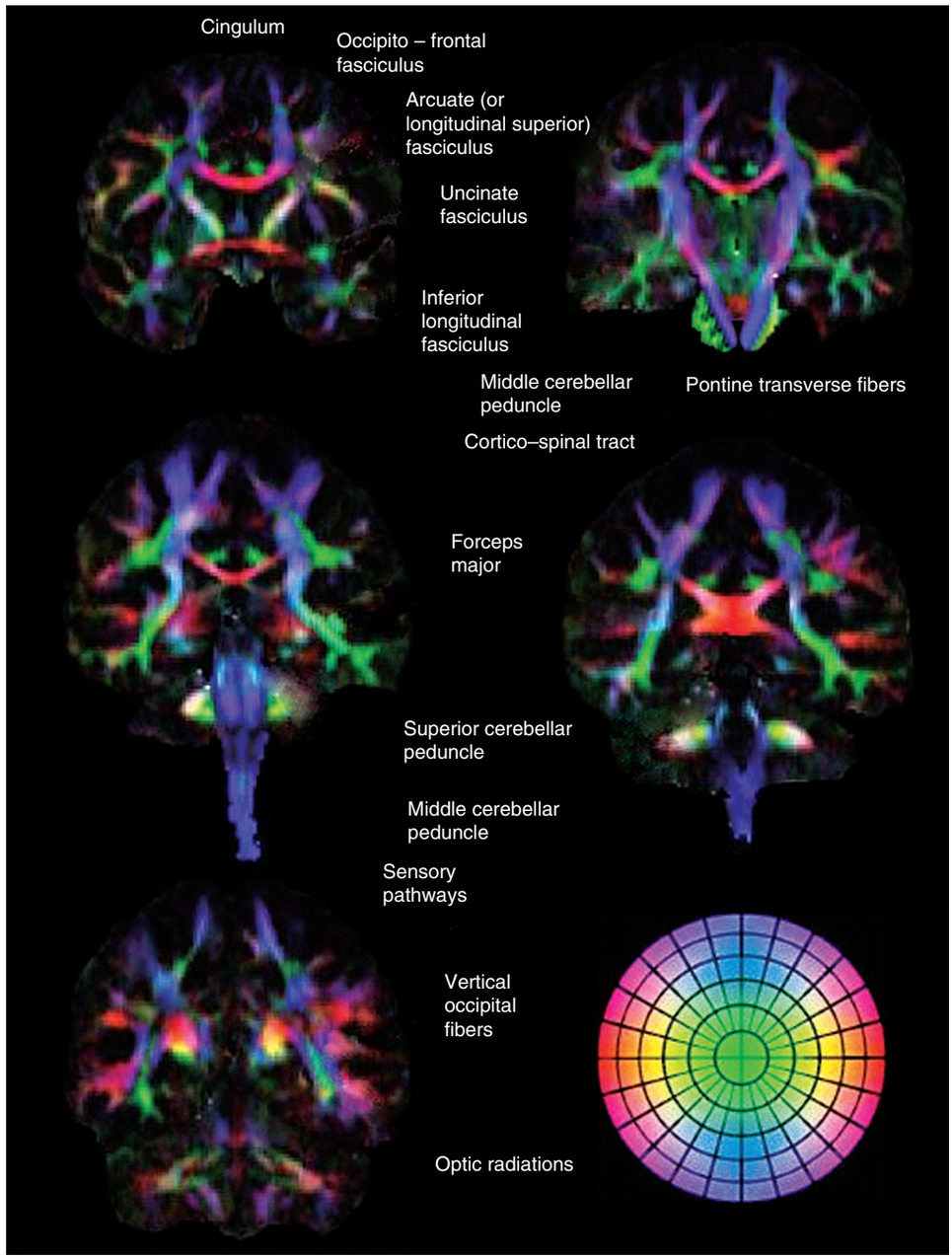

FIGURE 11-9

This direction-encoded color map depicts the major association, commissural, and projection pathways in the brain. *(From Pajevic S, Pierpaoli C: Color schemes to represent the orientation of anisotropic tissues from diffusion tensor data: application to white matter fiber tract mapping in the human brain. Magn Reson Med 42:526-540, 1999. Reproduced with permission of Wiley-Liss, Inc., a subsidiary of John Wiley & Sons, Inc.)*

much the same way fluid streamlines are generated from a fluid velocity field. Starting from a "seed point", fibers are launched in both directions until some stopping or "termination" criteria are satisfied, such as the *FA* drops below its level in background noise. A fiber tract consists of all points along such a continuous trajectory. One disadvantage of this computational strategy is that errors can accumulate during the tract following process. In general, it cannot be assured that the trajectories represent actual or even probable pathways of nerve fibers.

The second strategy is probabilistic in nature.[56-62] A seed point is assumed to be connected to all points within the imaging volume but the most probable connections are those that minimize some function, such as the strain energy of the pathway.[56] This approach holds great promise in that many paths are explored,

but only those that are frequently traversed are assigned a high likelihood. Of course, a disadvantage of this approach is that it is not known which physical constraints nature uses to construct nerve pathways. The development of probabilistic approaches that do not rely on such functional minimization appear to be quite promising,[63] but further validation studies still should be performed.

A hybrid tractography method, recently proposed by Jones and Pierpaoli,[64] uses the streamline in conjunction with an empirical statistical scheme such as bootstrapping. In this way, many possible paths can be generated from the same DWI data set and the variability of these paths can be assessed. This is done without making any assumptions about the source of artifacts in the DWIs. A disadvantage of this approach is that it generally requires acquiring more DWIs than is necessary for a typical DTI study.

It is important to note that a number of well-documented artifacts in DTI fiber tractography arise because a discrete, coarsely sampled, noisy, voxel-averaged direction field data,[49] are used to reconstruct topologically complex nerve pathways.[65] These artifacts can produce "phantom" connections between different brain regions that do not exist anatomically, or can result in missing anatomical connections that do exist. There are usually a number of thresholds and free parameters that can be set in existing tractography codes whose adjustment can alter the findings. Therefore, great care must be exercised both in obtaining "anatomical connectivity" obtained using DTI fiber tractography.[50] Clearly, some skepticism is warranted when interpreting such data—less in the coherent primary pathways, but increasingly in finer white matter structures.

Artful computer graphics-inspired schemes have been proposed to visualize fiber tract trajectories.[66] Zhang et al. have used stream tubes to visualize fiber tract trajectories and stream surfaces to visualize regions in which fibers cross within a plane.[67,68] An example of a stream tube representation of fiber tracts in the brain is given in Figure 11-10. These imaginative strategies will find increased use in displaying features of high-dimensional data inherent in DTI.

Stream tube visualization

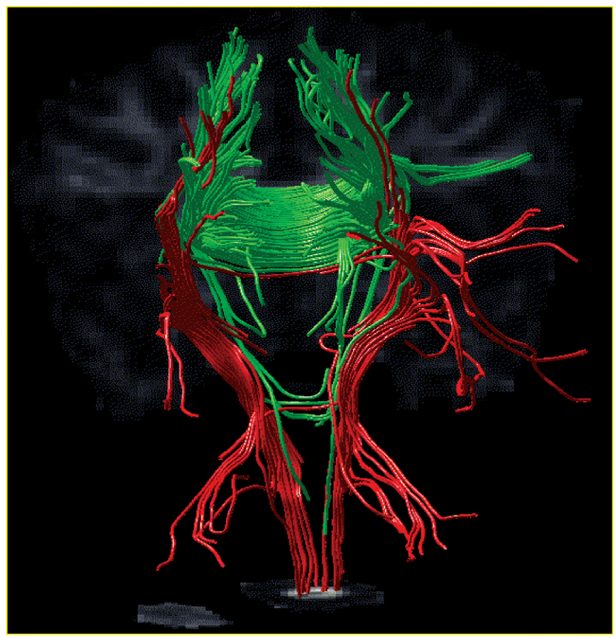

FIGURE 11-10

An example of computed fiber tracts in the brain. Here, fiber tracts are represented as "stream tubes," which are generated by following the direction of maximum diffusivity starting from "seedpoints" located in white matter ROIs. Novel computer visualization schemes such as this one will play an increasingly important role in representing the high-dimensional data contained in the diffusion tensor MRI data set. *(Courtesy of Derek Jones.)*

DWI ARTIFACTS

As seen earlier, DWI data is used to estimate D. Clearly any random or systematic artifacts in DWIs will adversely affect the estimate of D. Some of these artifacts have been discussed elsewhere in this book in Chapter 10 on DWI; however, many cause specific anomalies in DTI data, so they are described here as well. DWI artifacts are presented in order of importance as follows: Subject motion during the DWI acquisition can cause an artifactual redistribution of signal intensities within DWIs. Rigid body motion, such as rotation and translation are the easiest to correct for, since they involve applying a uniform phase offset to an entire image. This problem has been addressed by incorporating navigator echoes in the DWI pulse sequence.[69,70] More pernicious, however, is nonrigid body motion caused by eye movements, pulsations of CSF etc. At present, these artifacts cannot be entirely eliminated in DWIs, but they can be mitigated by the use of fast echo-planar DWI sequences and cardiac gating. Subject motion can also occur during the acquisition of a series of DWIs, like those used to estimate D. Recently a proposed remedy is to warp the set of DWIs to a common template using a nonrigid transformation that maximizes a measure of similarity among them.[71]

The large, rapidly switched magnetic field produced by the gradient coils during the diffusion sequence induces eddy currents in the conductive structures within the MRI scanner. These, in turn produce an additional unwanted, slowly decaying magnetic field. Two undesirable effects result: the field gradient at the sample differs from the prescribed field gradient (thus causing in a deviation from the prescribed b-matrix), and the slowly decaying field causes geometrical distortion of the DWI, which depends on the gradient strength and direction. These artifacts can adversely affect DTI studies because D is generally calculated in each voxel from a multiplicity of DWIs assuming that the prescribed gradients are the same as the gradients actually being applied to the tissue, and that each voxel contains the same tissue from scan to scan. Thus, uncompensated image distortion caused by eddy currents can lead to systematic errors in these estimated

diffusion parameters. Unfortunately, single-shot diffusion-weighted echo planar image (EPI) acquisitions are quite susceptible to eddy-current artifacts so correction schemes have to be used. One widely used strategy is to warp each DWI to a common template; another is to try to use a model of the effects of the eddy current on the phase map to correct it.[72] Nonrigid transformations of DWI data have recently been proposed to remedy this problem as well.[71]

Large discontinuities in the bulk magnetic susceptibility, such as those that occur at tissue-air interfaces produce local magnetic field gradients which are notorious for their contribution to image distortion, particularly during EPI. In addition to the image distortion, susceptibility variations within the brain adversely affect DWIs because the additional local gradients act like diffusion gradients, causing the b-matrix to be spatially varying. Fortunately, this effect appears to be limited to the volume of the brain adjacent to the sinuses.[73]

While at low levels of diffusion weighting the logarithm of the signal attenuation decreases linearly with increasing b-value, background noise causes the DWI intensity eventually to approach a baseline "noise floor" as the degree of diffusion weighting increases. Noise introduces an error in the estimated ADC or $\underline{D}$ when using Equations 1 or 2 in this regime. Background noise leads primarily to a bias in variance-based anisotropy measures of $\underline{D}$, (such as the *RA* and *FA*) as noise always introduces variability in the eigenvalues that makes isotropic media appear anisotropic, and anisotropic media appear more anisotropic.[32] Noise also biases the mean and variance of the corresponding eigenvectors of $\underline{D}$.[74] Unfortunately, the ability to characterize the deleterious effects of this artifact exceeds current understanding of how to remedy it,[32,75-77] although some recent work on the effects of background noise on DWIs has provided some new insights into how noise affects DTI measurements and how it can be ameliorated.[78]

The following problems can produce artifacts as well. Improper refocusing of rf pulses leads to added signal loss. Background gradients can be present because of improper shimming, which lead to additional signal attenuation if not properly compensated. This problem can often be remedied by measuring the background gradients directly[79] and incorporating them explicitly in the formula relating the signal intensity and the ADC or diffusion tensor. Flipping the signs of the diffusion gradients on alternate averages has been suggested as an aid in removing most cross-terms. Clearly, cross-terms arising between imaging gradients, albeit generally small, would not be corrected using this method. Moreover, averaging should be done on the logarithm of the intensity rather than the intensity, otherwise gradient cancellation will not occur. Gradient nonlinearity and miscalibration can lead to errors in the calculation of the ADC or $\underline{D}$ from a set of DWIs. The diffusion attenuation at different gradient strengths must be known for these formulae to provide meaningful results. If these gradients are not well calibrated, or they are not linear, signal attenuation observed in the image will be misattributed to diffusion processes in the sample. If the gradient in the x, y and z directions are coupled to one another (i.e., there is cross-talk) because of misalignment, then gradients applied in logical directions may have components in other directions. Such cross-talk could lead to problems, particularly in DTI.[80,81]

ISSUES IN INFERRING TISSUE MICROSTRUCTURE FROM NMR SIGNAL

Inferring the microstructure and underlying architectural organization of tissue using diffusion imaging data has been a long sought-after goal; however, its attainment is complicated by several factors. First, the homogeneity of tissue within each voxel cannot be assumed. Numerous microscopic compartments exist in brain parenchyma. Typically gray matter, white matter, and CSF can occupy the same voxel. The number of these distinct tissue types and their distribution within the voxel are generally not known a priori. At a microstructural level, gray and white matter are heterogeneous, having a distribution of macromolecular structures with a range of sizes, shapes, composition, and physical properties (such as T_2, D). Differences in relaxation parameters can lead to different rates of echo attenuation in each compartment, making it more difficult to explain the cause of signal loss within a voxel. There are also irregular boundaries between macromolecular and microscopic-scale compartments. Water diffusion may be restricted in some compartments and hindered in others. Some water will be associated with certain macromolecules while some will be free to diffuse. Another unknown is whether there is water exchange between compartments, which can also affect the relaxation rates of the spin system. Water movement within and between compartments is still not well understood, although tractable models exist to describe it. Owing to differences in blood flow and thermal conductivity, temperature cannot even be assumed to be uniform throughout a tissue sample. It is well known that temperature affects the measured diffusivity,[82-84] typically by about 1.5% for each degree (C).[84]

As an aside, the list given earlier in part explains why the underlying cause of diffusion anisotropy has not been fully elucidated in brain parenchyma, although at low b-values typical of DTI, most investigators ascribe it to ordered, heterogeneous structures, such as large oriented extracellular and intracellular macromolecules, super-macromolecular structures, organelles, and membranes. In the central nervous system, diffusion anisotropy is not simply caused by myelin in white matter, since it has been shown in several studies that even before myelin is deposited, diffusion anisotropy can be measured using MRI.[85-89] Thus, despite the fact that increases in myelin are temporally correlated with increases in diffusion anisotropy, structures other than the myelin sheath must also be contributing to diffusion anisotropy. This is important, because there is a common misconception that the degree of diffusion anisotropy can be used as a quantitative measure or "stain" of myelin content, when no such simple relationship exists.

Recently, with the advent of stronger magnetic field gradients, several groups have reported nonmonoexponential decay of the MR signal intensity as a function of b-value, e.g.,[90] and have attempted to infer from it properties of distinct tissue compartments. Putting aside the complexities of obtaining stable estimates of discrete exponentials (i.e., diffusion relaxography), numerous microstructural and architectural configurations could produce the same multi-exponential relaxation data. For example, Peled et al. showed that a system of impermeable tubes with a distribution of diameters consistent with those found in histological brain slices could give rise to multi-exponential decay of the signal.[91] Similar behavior is expected when there is a statistical distribution of any relevant physical property or microstructural dimension within a voxel. It is unlikely that a particular exponential in a multi-exponential model of diffusion attenuation can ever meaningfully be assigned to a particular and distinct tissue compartment. Clearly, without invoking additional a priori information about tissue structure, tissue composition, the physical properties of the different compartments, and their spatial distribution, determining tissue microstructural and architectural features from the NMR signal remains a challenging ill-posed inverse problem.

BEYOND DTI

DTI completely characterizes the Gaussian contribution of the water diffusion process within tissues.[92] Still, there is increasing evidence of restricted diffusion caused by water being trapped within regions bounded by impermeable barriers, which is described by a nonGaussian displacement profile, features of which several new methods have been proposed to characterize. These include diffusion spectrum imaging (DSI),[93] a variant of Callaghan's 3-D q-space MRI,[94] high angular resolution diffusion imaging (HARDI),[95,96] persistent angular structure MRI (PAS-MRI),[97] generalized diffusion-tensor MRI (GDTI),[98,99] Q-ball MRI,[100] composite hindered and restricted model of diffusion (CHARMED) MRI[101] and multi-tensor MRI.[102,103]

First, as a general requirement, all these methods must either subsume DTI or reduce to it in the limit of low b (or low q), where the Gaussian diffusion model applies.[92] Moreover, their experimental designs typically entail acquiring DWIs with a greater number of directions and/or a larger range of gradient strengths than are typically used in DTI. In principle, while one may obtain more information, it is generally at the price of additional acquisition time. In applications such as acute stroke monitoring, this price is unjustifiably high. In this case, it may be sufficient to produce a mean ADC or trace map, or even a DWI. In a careful neurological assessment of fiber tract organization in the brain, more information than DTI provides may be warranted. Clearly, the clinical or biological application determines the appropriate displacement imaging method used.

Another important point is that the methods mentioned earlier (including DTI) are all predicated on the assumption that each voxel in each DWI always contains the same tissue mass. While this assumption is not necessarily satisfied in DTI (although methods have been developed to correct this artifact), it is much less likely to be satisfied as the number of DWIs increases or as the b-value increases. Other forms of distortion (particularly eddy current distortion) can become severe at high b-values although some strategies have been proposed to ameliorate these.[104] At high b-values, however, bulk and small-scale motion are difficult to correct, since often there are few landmarks to identify in strongly diffusion-weighted images. Typically, since most of the signal attenuation is used to estimate $\underline{D}$ from the signal decay, little is left over to characterize the nonGaussian contribution. In this regime, noise becomes increasingly prominent in DWIs. The noise either has to be reduced or fitted in order not to introduce artifacts in the processed data. Recent work in the effects of noise in high b-value DWI is given in reference 78. Collectively these issues present serious technical challenges to all high b or high q methods, which will have to be ameliorated.

LONGITUDINAL AND MULTI-SITE STUDIES

In performing multi-site or longitudinal DTI studies, several additional issues arise. The most basic is how to compare high-dimensional $\underline{D}$ data obtained from different subjects or from the same subject at different times. This tensor data contains both scalar and vector information. Applying warping transformations developed only for scalar images, such as those implemented in statistical parametric mapping (SPM), produces nonsensical results when applied to DTI data without taking appropriate precautions to preserve the features of the tissue structure.[105] Current understanding of admissible transformations that can be applied to warp and register diffusion-tensor field data is still limited. A second issue is the proliferation of measures derived from $\underline{D}$ to characterize different features of isotropic and anisotropic diffusion. Consistent definitions of quantities such as the orientationally averaged diffusivity, *RA*, *FA*, etc. should be used. It is advisable to use the same imaging acquisition hardware, reconstruction software, and post-processing routines to help control for unnecessary variability. All sites should use a well-characterized phantom, even if it is isotropic, to ensure that no serious systematic artifacts exist, and that features of the DWIs are stable in time and among platforms.

Statistical analysis of DTI data is complicated by several factors. Although in an ideal DTI experiment, $\underline{D}$ has been shown to be distributed according to a multivariate normal distribution,[106] and Trace($\underline{D}$) has been shown to be distributed according to a univariate normal distribution,[107] the parametric distribution of many other tensor-derived parameters is unknown. Then, nonparametric statistical hypothesis testing methods should be used to determine whether an observed difference between different regions of interest (ROIs) is statistically significant. Empirical methods like the

bootstrap—which allow determination of the distribution of a statistical parameter empirically without knowledge of the form of its distribution a priori—show great promise in this application,[106] particularly now that a large number of single-shot DWIs can be acquired during a single scanning session, making this method practicable. Statistical properties of measured DTI parameters can then be compared on a voxel-by-voxel basis. Moreover, the bootstrap method can be used to assure data quality.

CONCLUSION

DTI provides a means to probe tissue structure at different levels of hierarchical organization. While experimental diffusion times are associated with water molecule displacements on the order of microns, these molecular motions are then averaged within a millimeter scale voxel, and then subsequently assembled into an image volume on a meter scale that encompasses tissues and organs. This integration permits us to study and elucidate complex structural features of tissue spanning length scales from the macromolecular to the macroscopic. Various DTI-derived parameters described earlier, such as maps of the eigenvalues of the diffusion tensor, its trace, measures of the degree of diffusion anisotropy and organization, estimates of fiber direction and white matter tract trajectory provide a unique multi-scale description of tissue architecture and organization.

Acknowledgment

Thanks go to Liz Salak, who edited this manuscript.

REFERENCES

1. Cleveland GG, Chang DC, Hazlewood CF, et al: Nuclear magnetic resonance measurement of skeletal muscle: anisotrophy of the diffusion coefficient of the intracellular water. Biophys J 16:1043-1053, 1976.
2. Tanner JE: Self diffusion of water in frog muscle. Biophys J 28:107-116, 1979.
3. Chenevert TL, Brunberg JA, Pipe JG: Anisotropic diffusion in human white matter: demonstration with MR techniques in vivo. Radiology 177:401-405, 1990.
4. Douek P, Turner R, Pekar J, et al: MR color mapping of myelin fiber orientation. J Comput Assist Tomogr 15:923-929, 1991.
5. Moseley ME, Kucharczyk J, Asgari HS, et al: Anisotropy in diffusion-weighted MRI. Magn Reson Med 19:321-326, 1991.
6. Sakuma H, Nomura Y, Takeda K, et al: Adult and neonatal human brain: diffusional anisotropy and myelination with diffusion-weighted MR imaging. Radiology 180:229-233, 1991.
7. Moonen CT, Pekar J, de Vleeschouwer MH, et al: Restricted and anisotropic displacement of water in healthy cat brain and in stroke studied by NMR diffusion imaging. Magn Reson Med 19:327-332, 1991.
8. Basser PJ, Mattiello J, Le Bihan D: MR diffusion tensor spectroscopy and imaging. Biophys J 66:259-267, 1994.
9. Garrido L, Wedeen VJ, Kwong KK, et al: Anisotropy of water diffusion in the myocardium of the rat. Circ Res 74:789-793, 1994.
10. Turner R, Le Bihan D, Maier J, et al: Echo-planar imaging of intravoxel incoherent motion. Radiology 177:407-414, 1990.
11. Moseley ME, Cohen Y, Kucharczyk J, et al: Diffusion-weighted MR imaging of anisotropic water diffusion in cat central nervous system. Radiology 176:439-445, 1990.
12. Henkelman RM, Stanisz GJ, Kim JK, et al: Anisotropy of NMR properties of tissues: Anisotropy of NMR properties of tissues. Magn Reson Med 32:592-601, 1994.
13. Crank J: The mathematics of diffusion, 2nd ed. Oxford: Oxford University Press, 1975.
14. Basser PJ, Mattiello J, Le Bihan D: Estimation of the effective self-diffusion tensor from the NMR spin echo. J Magn Reson B 103:247-254, 1994.
15. Mattiello J, Basser PJ, Le Bihan D: Analytical expression for the b matrix in NMR diffusion imaging and spectroscopy. J Magn Reson A 108:131-141, 1994.
16. Mattiello J, Basser PJ, Le Bihan D: The b matrix in diffusion tensor echo-planar imaging. Magn Reson Med 37, 292-300, 1997.
17. Mattiello J, Basser PJ, Le Bihan D: Analytical calculation of the b matrix in diffusion imaging. In Bihan DL (ed): Diffusion and Perfusion Magnetic Resonance Imaging. New York: Raven Press, 77-90, 1995.
18. Stejskal EO, Tanner JE: Spin diffusion measurements: spin echoes in the presence of time-dependent field gradient. J Chem Phys 42:288-292, 1965.
19. Neeman M, Freyer JP, Sillerud LO: Pulsed-gradient spin-echo studies in NMR imaging. Effects of the imaging gradients on the determination of diffusion coefficients. J Magn Reson 90:303-312, 1990.
20. Basser PJ, Mattiello J, Le Bihan D: In 11th Annual Meeting of the SMRM, Berlin. 1:1222, 1992.
21. Einstein A: Investigations on the Theory of the Brownian Movement. New York: Dover Publications, 1926.
22. Stejskal EO: Use of spin echoes in a pulsed magnetic field gradient to study restricted diffusion and flow. J Chem Phys 43:3597-3603, 1965.
23. Basser PJ, Le Bihan D: In 11th Annual Meeting of the SMRM, Berlin. 1:1221, 1992.
24. Basser PJ, Mattiello J, Pierpaoli C, Le Bihan D: In IEEE 16th Annual International Meeting of the IEEE EMBS, Baltimore. 445, 1994.
25. Kärger J, Pfeifer H, Heink W. In Waugh J (ed): Advances in Magnetic Resonance. New York: Academic Press, 12: 1-89, 1988.
26. Moseley ME, Kucharczyk J, Mintorovitch J, et al: Diffusion-weighted MR imaging of acute stroke: correlation with T2-weighted and magnetic susceptibility-enhanced MR imaging in cats. Am J Neuroradiol 11:423-429, 1990.
27. Moseley ME, Mintorovitch J, Cohen Y, et al: Early detection of ischemic injury: comparison of spectroscopy, diffusion-, T2-, and magnetic susceptibility-weighted MRI in cats. Acta Neurochir Suppl (Wien) 51:207-209, 1990.
28. Moseley ME, Cohen Y, Mintorovitch J, et al: Early detection of regional cerebral ischemia in cats: comparison of diffusion- and T2-weighted MRI and spectroscopy. Magn Reson Med 14:330-346, 1990.
29. Warach S, Gaa J, Siewert B, et al: Acute human stroke studied by whole brain echo planar diffusion-weighted magnetic resonance imaging. Ann Neurol 37:231-241, 1995.
30. Warach S, Chien D, Li W, et al: Fast magnetic resonance diffusion-weighted imaging of acute human stroke. Neurology 42:1717-1723, 1992.
31. Doran M, Hajnal JV, Van Bruggen N, et al: Normal and abnormal white matter tracts shown by MR imaging using directional diffusion weighted sequences. J Comput Assist Tomogr 14:865-873, 1990.
32. Pierpaoli C, Basser PJ: Toward a quantitative assessment of diffusion anisotropy. Magn Reson Med 36:893-906, 1996.
33. Pierpaoli C, Jezzard P, Basser PJ, et al: Diffusion tensor MR imaging of the human brain. Radiology 201:637-648, 1996.
34. Ulug AM, Beauchamp N, Bryan RN, van Zijl PCM: Absolute quantitation of diffusion constants in human stroke. Stroke 28:483-490, 1997.
35. van Gelderen P, de Vleeschouwer MHM, DesPres D, et al: Water diffusion and acute stroke. Magn Reson Med 31:154-163, 1994.
36. Wong EC, Cox RW, Song AW: Optimized isotropic diffusion weighting. Magn Reson Med 34:139-143, 1995.
37. Mori S, van Zijl PC: Diffusion weighting by the trace of the diffusion tensor within a single scan. Magn Reson Med 33:41-52, 1995.
38. Basser PJ, Jones DK: Diffusion-tensor MRI: theory, experimental design and data analysis — a technical review. NMR Biomed 15:456-467, 2002.
39. Basser PJ: Inferring microstructural features and the physiological state of tissues from diffusion-weighted images. NMR Biomed 8:333-344, 1995.
40. Basser PJ, Pierpaoli C: Microstructural and physiological features of tissues elucidated by quantitative-diffusion-tensor MRI. J Magn Reson B 111:209-219, 1996.
41. Shimony JS, McKinstry RC, Akbudak E, et al: Quantitative diffusion-tensor anisotropy brain MR imaging: normative human data and anatomic analysis. Radiology 212:770-784, 1999.
42. Westin CF, Maier S, Khidir B, et al: In *MICCAI'99*; Cambridge: Springer-Verlag: LNCS-1679:441-452, 1999.
43. Pajevic S, Aldroubi A, Basser PJ: A continuous tensor field approximation of discrete DT-MRI data for extracting microstructural and architectural features of tissue. J Magn Reson 154:85-100, 2002.
44. Poupon C, Clark CA, Frouin V, et al: Regularization of diffusion-based direction maps for the tracking of brain white matter fascicles. Neuroimage 12:184-195, 2000.
45. Pajevic S, Pierpaoli C: Color schemes to represent the orientation of anisotropic tissues from diffusion tensor data: application to white matter fiber tract mapping in the human brain. Magn Reson Med 42:526-540, 1999.
46. Makris N, Worth AJ, Sorensen AG, et al: Morphometry of in vivo human white matter association pathways with diffusion-weighted magnetic resonance imaging. Ann Neurol 42:951-962, 1997.
47. Pajevic S, Pierpaoli C: Color schemes to represent the orientation of anisotropic tissues from diffusion tensor data: application to white matter fiber tract mapping in the human brain. Magn Reson Med 43:921, 2000.

48. Wedeen VJ, Davis TL, Weisskoff RM, et al: In Proceedings of the First International Conference for Functional Mapping of the Human Brain, Paris, 1:36, 1995.
49. Basser PJ: In 6th Annual Meeting of the ISMRM, Sydney, 2:1226, 1998.
50. Basser PJ, Pajevic S, Pierpaoli C, et al: In vivo fiber tractography using DT-MRI data. Magn Reson Med 44:625-632, 2000.
51. Conturo TE, Lori NF, Cull TS, et al: Tracking neuronal fiber pathways in the living human brain. Proc Natl Acad Sci U S A 96:10422-10427, 1999.
52. Mori S, Crain BJ, Chacko VP, et al: Three-dimensional tracking of axonal projections in the brain by magnetic resonance imaging. Ann Neurol 45:265-269, 1999.
53. Poupon C, Clark CA, Frouin V, et al: In 8th Annual Meeting of the ISMRM: Philadelphia, 325, 1999.
54. Jones DK, Simmons A, Williams SC, et al: Non-invasive assessment of axonal fiber connectivity in the human brain via diffusion tensor MRI. Magn Reson Med 42:37-41, 1999.
55. Bammer R, Acar B, Moseley ME: In vivo MR tractography using diffusion imaging. Eur J Radiol 45:223-234, 2003.
56. Tuch DS, Belliveau JW, Wedeen V: In Eighth Annual Meeting of the ISMRM, ISMRM, Berkeley, CA. 791, 2000.
57. Parker GJ, Haroon HA, Wheeler-Kingshott CA: A framework for a streamline-based probabilistic index of connectivity (PICo) using a structural interpretation of MRI diffusion measurements. J Magn Reson Imaging 18:242-254, 2003.
58. Koch M, Glauche V, Finsterbusch J, et al: Estimation of anatomical, connectivity from diffusion tensor data. *NeuroImage* 13:S176, 2001.
59. Koch MA, Norris DG, Hund-Georgiadis M: An investigation of functional and anatomical connectivity using magnetic resonance imaging. Neuroimage 16:241-250, 2002.
60. Batchelor PG, Hill DLG, Calamante F, Atkinson D: In 17th International Conference, IMPI'01; Information Processing in Medical Imaging 121-133, 2001.
61. Parker GJ, Wheeler-Kingshott CA, Barker GJ: Estimating distributed anatomical connectivity using fast marching methods and diffusion tensor imaging. IEEE Trans Med Imaging 21:505-512, 2002.
62. Behrens TEJ, Jenkinson M, Brady JM, Smith SM: In ISMRM: Honolulu. 1142, 2002.
63. Behrens TE, Woolrich MW, Jenkinson M, et al: Characterization and propagation of uncertainty in diffusion-weighted MR imaging. Magn Reson Med 50:1077-1088, 2003.
64. Jones DK, Pierpaoli C: In 12th Annual ISMRM: Kyoto, Japan. 2004.
65. Pierpaoli C, Barnett A, Pajevic S, et al: Water diffusion changes in Wallerian degeneration and their dependence on white matter architecture. Neuroimage 13:1174-1185, 2001.
66. Catani M, Howard RJ, Pajevic S, Jones DK: Virtual in vivo interactive dissection of white matter fasciculi in the human brain. Neuroimage 17:77-94, 2002.
67. Zhang S, Curry C, Morris DS, Laidlaw DH: In Proceedings of the IEEE Visualization Conference: Utah, 2000
68. Zhang S, Bastin ME, Laidlaw DH, et al: Visualization and analysis of white matter structural asymmetry in diffusion tensor MRI data. Magn Reson Med 51:140-147, 2004.
69. Anderson AW, Gore JC: Analysis and correction of motion artifacts in diffusion weighted imaging. Magn Reson Med 32:379-387, 1994.
70. Ordidge RJ, Helpern JA, Qing ZX, et al: Correction of motional artifacts in diffusion-weighted MR images using navigator echoes. Magn Reson Imaging 12:455-460, 1994.
71. Rohde GK, Barnett AS, Basser PJ, et al: Comprehensive approach for correction of motion and distortion in diffusion-weighted MRI. Magn Reson Med 51:103-114, 2004.
72. Jezzard P, Barnett AS, Pierpaoli C: Characterization of and correction for eddy current artifacts in echo planar diffusion imaging. Magn Reson Med 39:801-812, 1998.
73. Clark CA, Barker GJ, Tofts PS: Improved reduction of motion artifacts in diffusion imaging using navigator echoes and velocity compensation. J Magn Reson 141:52-61, 1999.
74. Basser PJ, Pajevic S: Statistical artifacts in diffusion tensor MRI (DT-MRI) caused by background noise. Magn Reson Med 44:41-50, 2000.
75. Martin KM, Papadakis NG, Huang CL, et al: The reduction of the sorting bias in the eigenvalues of the diffusion tensor. Magn Reson Imaging 17:893-901, 1999.
76. Basser PJ, Pajevic S: Statistical artifacts in diffusion tensor MRI (DT-MRI) caused by background noise. Magn Reson Med 44:41-50, 2000.
77. Basser PJ, Pajevic S: In 7th Annual ISMRM: Philadelphia, 1788, 1999.
78. Jones DK, Basser PJ: Squashing peanuts and smashing pumpkins. How noise distorts diffusion-weighted MR data. Magn Reson Med 52:979-993, 2004.
79. Jara H, Wehrli FW: Determination of background gradients with diffusion MR imaging. J Magn Reson Imaging 4:787-797, 1994.
80. Basser PJ: In Third Meeting of the SMR: Nice, France, 308, 1995.
81. Basser PJ, Mattiello J, Le Bihan D: Method and system for measuring the diffusion tensor and for diffusion tensor imaging. USPTO 5:529-531, 1996.
82. Le Bihan D, Delannoy J, Levin RL: Temperature mapping with MR imaging of molecular diffusion: application to hyperthermia. Radiology 171:853-857, 1989.
83. Mills R: Sef-diffusion in normal and heavy water in the range 1–45°. Journal of Physical Chemistry 77:685-688, 1973.
84. Simpson JH, Carr HY: Diffusion and nuclear spin relaxation in water. Physical Review 111:1201-1202, 1958.
85. Neil JJ, Shiran SI, McKinstry RC, et al: Normal brain in human newborns: apparant diffusion coefficient and diffusion anistropy measured by using diffusion tensor MR imaging. Radiology 209:57-66, 1998.
86. Beaulieu C, Allen PS: Water diffusion in the giant axon of the squid: implications for diffusion-weighted MRI of the nervous system. Magn Reson Med 32:579-583, 1994.
87. Beaulieu C, Allen PS: Determinants of anisotropic water diffusion in nerves. Magn Reson Med 31:394-400, 1994.
88. Wimberger DM, Roberts TP, Barkovich AJ, et al: Identification of "premyelination" by diffusion-weighted MRI. J Comput Assist Tomogr 19:28-33, 1995.
89. Beaulieu C: The basis of anisotropic water diffusion in the nervous system – a technical review. NMR Biomed 15:435-455, 2002.
90. Mulkern RV, Gudbjartsson H, Westin CF, et al: Multi-component apparent diffusion coefficients in human brain. NMR Biomed 12:51-62, 1999.
91. Peled S, Cory DG, Raymond SA, et al: Water diffusion, T(2), and compartmentation in frog sciatic nerve. Magn Reson Med 42:911-918, 1999.
92. Basser PJ: Relationships between diffusion tensor and q-space MRI. Magn Reson Med 47:392-397, 2002.
93. Wedeen VJ, Reese TG, Tuch DS, et al: In 8th Annual Meeting of the ISMRM: Denver, 82, 2000.
94. Callaghan PT. Principles of nuclear magnetic resonance microscopy. Oxford: Oxford University Press, 1991.
95. Frank LR: Characterization of anisotropy in high angular resolution diffusion-weighted MRI. Magn Reson Med 47:1083-1099, 2002.
96. Frank LR: Anisotropy in high angular resolution diffusion-weighted MRI. Magn Reson Med 45:935-939, 2001.
97. Jansons KM, Alexander DC: Persistent angular structure: new insights from diffusion magnetic resonance imaging data. Inverse Probl 19:1031-1046, 2003.
98. Ozarslan E, Mareci TH: Generalized diffusion tensor imaging and analytical relationships between diffusion tensor imaging and high angular resolution diffusion imaging. Magn Reson Med 50:955-965, 2003.
99. Liu CL, Bammer R, Moseley ME: Generalised diffusion tensor imaging (GDTI): a method for characterising and imaging diffusion anistropy caused by non-Gaussian diffusion. Israel J Chem 43:145-154, 2003.
100. Tuch DS, Reese TG, Wiegell MR, et al: Diffusion MRI of complex neural architecture. Neuron 40:885-895, 2003.
101. Assaf Y, Freidlin RZ, Rohde GK, et al: New modeling and experimental framework to characterize hindered and restricted water diffusion in brain white matter. Magn Reson Med 52:965-978, 2004.
102. Inglis BA, Bossart EL, Buckley DL, et al: Visualization of neural tissue water compartments using biexponential diffusion tensor MRI. Magn Reson Med 45:580-587, 2001.
103. Clark CA, Le Bihan D: Water diffusion compartmentation and anisotropy at high b values in the human brain. Magn Reson Med 44:852-859, 2000.
104. Reese TG, Heid O, Weisskoff RM, et al: Reduction of eddy-current-induced distortion in diffusion MRI using a twice-refocused spin echo. Magn Reson Med 49: 177-182, 2003.
105. Alexander DC, Pierpaoli C, Basser PJ, et al: Spatial transformations of diffusion tensor magnetic resonance images. IEEE Trans Med Imaging 20:1131-1139, 2001.
106. Pajevic S, Basser PJ: Parametric and non-parametric statistical analysis of DT-MRI data. J Magn Reson 161:1-14, 2003.
107. Basser PJ, Pajevic S: Dealing with uncertainty in DT-MRI data. Israel J Chem 43:129-144, 2003.